Spatial Domain Method for the Design of RF Pulses in Multicoil Parallel Excitation

William Grissom,[1*] Chun-yu Yip,[2] Zhenghui Zhang,[3] V. Andrew Stenger,[4] Jeffrey A. Fessler,[1,2] and Douglas C. Noll[1]

Parallel excitation has been introduced as a means of accelerating multidimensional, spatially-selective excitation using multiple transmit coils, each driven by a unique RF pulse. Previous approaches to RF pulse design in parallel excitation were either formulated in the frequency domain or restricted to echo-planar trajectories, or both. This paper presents an approach that is formulated as a quadratic optimization problem in the spatial domain and allows the use of arbitrary *k*-space trajectories. Compared to frequency domain approaches, the new design method has some important advantages. It allows for the specification of a region of interest (ROI), which improves excitation accuracy at high speedup factors. It allows for magnetic field inhomogeneity compensation during excitation. Regularization may be used to control integrated and peak pulse power. The effects of Bloch equation nonlinearity on the large-tip-angle excitation error of RF pulses designed with the method are investigated, and the utility of Tikhonov regularization in mitigating this error is demonstrated. Magn Reson Med 56: 620–629, 2006. © 2006 Wiley-Liss, Inc.

Key words: transmit SENSE; parallel excitation; pulse design; selective excitation; large-tip-angle excitation

Parallel excitation was recently proposed (1,2) as a means of accelerating multidimensional selective excitation using multiple coils driven with independent waveforms. In a manner analogous to parallel imaging methods, such as sensitivity encoding (SENSE) (4) and generalized autocalibrating partially parallel acquisition (GRAPPA) (5), a reduced excitation *k*-space trajectory (6) can be used to achieve a desired excitation pattern by exploiting the blurring behavior of coil sensitivity patterns in the excitation *k*-space domain to deposit RF energy in regions that are not traversed by the trajectory. Accelerated selective excitation is useful for reducing specific absorption rate (SAR) (2), and shortening multidimensional RF pulses in such applications as compensation for B_1 and B_0 inhomogeneity (7–10). The feasibility of parallel excitation was also recently verified experimentally (11,12).

Several methods currently exist for designing small-tip-angle RF pulses in parallel excitation (1–3). The pioneering pulse design methods were introduced by Katscher et al. (1) and Zhu (2). The method introduced by Katscher et al. (1), dubbed transmit SENSE, is characterized by the explicit use of transmit sensitivity patterns in the pulse design process, and its formulation is based on a convolution in excitation *k*-space. It allows usage of arbitrary *k*-space trajectories. Zhu's (2) method makes explicit use of transmit sensitivity patterns, but is formulated as an optimization problem in the spatial domain, and, as described, is restricted to echo-planar *k*-space trajectories. Griswold et al. (3) proposed a *k*-space domain method that is analogous to GRAPPA imaging. It is unique in that it does not require prior determination of sensitivity patterns. Instead, it involves an extra calibration step in the pulse design process. It also appears to be restricted to echo-planar *k*-space trajectories.

In this paper we propose an alternative RF pulse design method that is closely related to transmit SENSE (1), but is formulated in the spatial domain. It is a multicoil generalization of the iterative pulse design method proposed by Yip et al. (13), and is based on the minimization of a quadratic cost function that consists of an excitation error term, which quantifies excitation error in the spatial domain, and a choice of regularization terms. The regularization terms can be used to control the integrated and peak RF power. The minimization problem can be solved iteratively via the conjugate gradient (CG) method (14) or brute-force inversion. We demonstrate that the new approach is approximately equivalent to that described in Ref. 1 under special conditions, but it has several new advantages. It allows for spatially variant excitation error weighting and thus region of interest (ROI) specification. Main field inhomogeneity is easily incorporated in the design. Unlike Katscher et al.'s (1) method, it does not require computation of a Jacobian determinant for compensation of *k*-space velocity and density, nor does it require interpolation between excitation *k*-space trajectories.

To date, all RF pulse design methods for parallel excitation are based on the assumption of small-tip-angle excitation. Beyond the small-tip-angle regime, it is expected that the nonlinearity of the Bloch equation will have an adverse effect on the performance of pulses designed using these methods. Because it is often desirable to use large-tip-angle pulses, we investigated the behavior, in terms of excitation error, of pulses designed using the proposed spatial domain method as they are scaled to produce relatively large tip angles (up to 90°). We also investigated the utility of Tikhonov regularization on integrated pulse power (13) for mitigating this error.

[1]Department of Biomedical Engineering, University of Michigan, Ann Arbor, Michigan, USA.

[2]Department of Electrical Engineering and Computer Science, University of Michigan, Ann Arbor, Michigan, USA.

[3]Department of Bioengineering, University of Pittsburgh, Pittsburgh, Pennsylvania, USA.

[4]Department of Medicine, University of Hawaii, Manoa, Hawaii, USA.

Grant sponsor: NIH; Grant number: DA15410.

*Correspondence to: William Grissom, Functional MRI Laboratory, University of Michigan, 2360 Bonisteel Ave., Ann Arbor, MI 48109-2108. E-mail: wgrissom@umich.edu

Received 29 September 2005; revised 28 April 2006; accepted 2 May 2006.
DOI 10.1002/mrm.20978
Published online 7 August 2006 in Wiley InterScience (www.interscience.wiley.com).

In the following section we formulate small-tip-angle RF pulse design for multicoil parallel excitation in the spatial domain as an optimization problem. We then present Bloch equation simulation results that show quantitatively the benefits of the proposed method, in terms of excitation accuracy, at high speedup factors or when off-resonance is present. We then present the results of our investigation into the large-tip-angle behavior of pulses designed using the spatial domain method. Finally, we present experimental results validating our design technique using a method we developed that exploits the linearity of small-tip-angle excitation and the MR signal equation to swap the roles of transmitters and receivers.

THEORY

The spatial domain design approach is an extension of the single-coil iterative RF pulse design method introduced by Yip et al. (13). Assuming small tip angles, the transverse plane excitation pattern produced by a single coil can be approximated by the Fourier integral of an excitation *k*-space trajectory (10), $\mathbf{k}(t) = [k_x(t)\ k_y(t)\ k_z(t)]$, weighted by a complex RF pulse $b(t)$ and spatially weighted by the coil's complex transmit sensitivity $s(\mathbf{x})$:

$$m(\mathbf{x}) = i\gamma m_0 s(\mathbf{x}) \int_0^T b(t) e^{i\gamma \Delta B_0(\mathbf{x})(t-T)} e^{i\mathbf{x}\cdot\mathbf{k}(t)} dt, \qquad [1]$$

where γ is the gyromagnetic ratio, m_0 is the equilibrium magnetization magnitude, T is the pulse length, and $e^{i\gamma\Delta B_0(\mathbf{x})(t-T)}$ represents the phase accrued due to main field inhomogeneity defined by the field map $\Delta B_0(\mathbf{x})$. The trajectory $\mathbf{k}(t)$ is defined as the time-reversed integration of the gradient waveforms (10). Exploiting linearity in the small-tip-angle regime, the excitation patterns from multiple coils can be spatially superposed to form an aggregate pattern:

$$m(\mathbf{x}) = i\gamma m_0 \sum_{r=1}^{R} s_r(\mathbf{x}) \int_0^T b_r(t) e^{i\gamma \Delta B_0(\mathbf{x})(t-T)} e^{i\mathbf{x}\cdot\mathbf{k}(t)} dt, \qquad [2]$$

where R is the number of transmit coils, each with sensitivity pattern $s_r(\mathbf{x})$ and unique RF pulse $b_r(t)$. Discretizing time to N_t samples and space to N_s samples, we may write:

$$\mathbf{m} = \sum_{r=1}^{R} \mathbf{D}_r \mathbf{A}\, \mathbf{b}_r, \qquad [3]$$

where $\mathbf{m}$ is the length-N_s vector of spatial samples of the aggregate excitation pattern, $\mathbf{D}_r = diag\{s_r(\mathbf{x}_i)\}$ is a diagonal matrix containing samples of the sensitivity pattern of coil r, and $\mathbf{b}_r$ is a length- N_t vector of RF pulse samples for coil r. The (i, j)-th element of the $N_s \times N_t$ system matrix $\mathbf{A}$ is given by:

$$a_{ij} = i\gamma m_0 \Delta t e^{i\gamma \Delta B_0(\mathbf{x}_i)(t_j - T)} e^{i\mathbf{x}_i\cdot\mathbf{k}(t_j)}. \qquad [4]$$

Equation [3] can be rewritten via horizontal concatenation of the matrices $\mathbf{D}_r\mathbf{A}$ and vertical concatenation of the vectors $\mathbf{b}_r$, resulting in:

$$\mathbf{m} = \begin{bmatrix} \mathbf{D}_1\mathbf{A} & \cdots & \mathbf{D}_R\mathbf{A} \end{bmatrix} \begin{bmatrix} \mathbf{b}_1 \\ \vdots \\ \mathbf{b}_R \end{bmatrix} = \mathbf{A}_{full}\mathbf{b}_{full}. \qquad [5]$$

Given a vector $\mathbf{m}_{des}$ containing N_s samples of a desired pattern at the spatial locations $\mathbf{x}_i$, the RF pulses can be designed via solving the following minimization problem:

$$\hat{\mathbf{b}}_{full} = \arg\min_{\mathbf{b}_{full}} \{\|\mathbf{A}_{full}\mathbf{b}_{full} - \mathbf{m}_{des}\|_{\mathbf{W}}^2 + R(\mathbf{b}_{full})\}, \qquad [6]$$

where $\mathbf{W}$ is an $N_s \times N_s$ diagonal matrix containing a spatial error weighting that one can use to specify spin-free regions as "don't-care" regions, and $R(\mathbf{b}_{full})$ denotes a general regularization term that is a function of the RF samples. Integrated RF power may be controlled via a Tikhonov regularization term $R(\mathbf{b}_{full}) = \beta\mathbf{b}'_{full}\mathbf{b}_{full}$, where prime denotes complex conjugate transpose, and β is a tuning parameter. As shown later in this work, this term is useful for mitigating increased excitation error when RF pulses are scaled to achieve large tip angles. Peak RF power may be controlled via $R(\mathbf{b}_{full}) = \mathbf{b}'_{full}\Lambda\mathbf{b}_{full}$, where $\Lambda = diag(\lambda_j)$, with λ_j, $j = 0, \ldots, R \cdot N_t - 1$, denoting regularization parameters used to control the magnitude of individual RF pulse samples (13). The minimization problem can be solved by brute-force inversion or efficiently by the CG method, in a manner similar to the single-coil pulse design method proposed in Ref. 13.

In the special case in which a field map is not incorporated into the system matrix, error weighting is not specified, and Tikhonov regularization is used, our proposed method and the frequency domain approach of transmit SENSE (1) are approximately equivalent (see Appendix). However, in general, our method offers the extra advantages of ROI specification via the $\mathbf{W}$ matrix, and better system modeling via field map incorporation in the system matrix $\mathbf{A}$, which improve excitation accuracy. Computation is also reduced compared to the frequency domain method because there is no need in our method to transform the desired pattern and sensitivity patterns to the frequency domain, nor does it require computation of a Jacobian determinant for *k*-space sampling density and velocity compensation, or interpolation between *k*-space trajectories.

MATERIALS AND METHODS

Pulse Design

RF pulses were computed in MATLAB 7.0.4 (MathWorks, Inc., Natick, MA), on a 2.0 GHz Pentium 4 computer with 1 Gb of RAM, using the CG algorithm initialized with a zero pulse and run for 60 iterations (13,14). Except in Simulation III, no Tikhonov regularization was used. In all cases a single-shot spiral-out excitation *k*-space trajectory was used with the following parameters: maximum amplitude = 4 G/cm, maximum slew rate = 18000 G/cm/s, and sampling period 4 μs. To accelerate excitation, we used

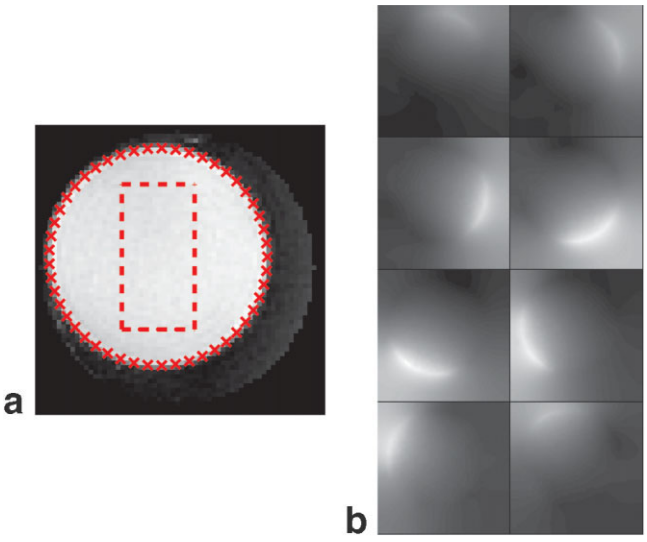

FIG. 1. **a:** The ROI mask (dashed circle) for NRMSE calculation and pulse design was obtained by thresholding the body coil image of a phantom. The desired excitation pattern (dashed rectangle) was centered in the ROI, with uniform tip angle, zero phase, and dimensions 5 cm × 10 cm. **b:** Receive coil sensitivity patterns (magnitude) of an eight-channel head array, as measured on a spherical phantom. These patterns are used in the numerical simulations of parallel excitation.

trajectories that radially undersampled *k*-space, resulting in reduction of the excitation field of view (XFOV) of individual coils' excitation patterns. We define the "speedup factor" as the ratio of the FOV of the desired pattern to the reduced XFOV of the individual coils' excitation patterns. This convention is adopted because, regardless of *k*-space trajectory used, acceleration in parallel excitation is always achieved via undersampling in the FOV dimension. Alternative definitions, such as the ratio of unaccelerated and accelerated pulse lengths, would make it more difficult to conduct performance comparisons across *k*-space trajectories, since the savings in pulse length would be specific to the trajectory used and the hardware on which it was implemented. *k*-Space trajectories were chosen to achieve a spatial resolution of 0.625 cm. The desired excitation pattern (Fig. 1a) was a 5 × 10 cm rectangle of uniform tip angle (magnitude 0.1, corresponding to tip angle of 6°) and zero phase. The pattern was defined on a 64 × 64 Cartesian grid in a 20 × 20 cm region.

To obtain transmit sensitivity patterns, we estimated the receive sensitivity patterns (Fig. 1b) of an eight-channel head coil array (MRI Devices), and made the assumption that the resulting patterns represented reasonable transmit sensitivity patterns, though perhaps not exactly those of the head array coil used. The sensitivity patterns were estimated by imaging a spherical phantom with a gradient-echo (GRE) spiral sequence with a slice-selective sinc pulse, using both the head coil array and the body coil. The head coil array images were divided by the body coil image, and then smoothed in an iterative penalized least-squares fashion, as described in Ref. 15, to yield the final sensitivity patterns. Nonzero coil sensitivity outside the phantom can be attributed to the smoothing operation in the sensitivity estimation process. The body coil image was thresholded (at 0.3 of its maximum magnitude) to derive an ROI (Fig. 1a) that defined a spatial error weighting function in which the "care" region had error weighting 1, and the "don't care" region outside the ROI had error weighting 0.

Numerical Simulations

We performed Bloch equation simulations to test the pulse design methods. Simulations were performed over a 128 × 128 transverse grid covering a 20 cm × 20 cm region. Relaxation effects were ignored. Normalized root-mean-square excitation error (NRMSE) was calculated for each result from the Bloch simulator ($\mathbf{m}_{bl}$). It was defined as $\|\mathbf{m}_{bl} - \mathbf{d}_{bl}\|_{\mathbf{w}_{bl}}/\|\mathbf{d}_{bl}\|_{\mathbf{w}_{bl}}$, where $\mathbf{d}_{bl}$ and $\mathbf{W}_{bl}$ are the desired pattern and error weighting interpolated to the Bloch simulation grid, respectively. The ROI for NRMSE calculation was the same as that used in pulse design. We also obtained the transmit sensitivity patterns used in the simulation by interpolating those used in the pulse design.

Simulation I: Off-Resonance Correction

In simulation I we evaluated the ability of our design method to correct for off-resonance during excitation. In the Bloch simulator we incorporated a field map with flat regions in the center (+150 Hz) and background (0 Hz), bridged by a linear transition region (Fig. 2a). The frequency offset of the center region represents a typical field map value at 3T. We compared the performance of our method with and without field map incorporation to the performance of pulses designed with the frequency domain method of transmit SENSE (1), in terms of NRMSE within the ROI. The applied spiral trajectory radially undersampled *k*-space, yielding a speedup factor of 2 and a pulse length of 3.8 ms.

Simulation II: Speedup Factor

In simulation II we tested our design method's performance as a function of speedup factor, with and without ROI specification, and compared this with the performance of pulses designed with the frequency domain method. NRMSE was calculated over the ROI. The speedup factor was varied from one, corresponding to no reduction in XFOV, to 20, corresponding to a 20-fold reduction in XFOV. As the speedup factor was incremented from 1 to 20, pulse length was reduced from 6.9 ms to 0.25 ms.

Simulation III: Tip Angle

In simulation III we studied the relationships among the speedup factor, Tikhonov regularization, and excitation accuracy of RF pulses at large tip angles. For a given speedup factor and Tikhonov regularization parameter value β, we designed RF pulses using our spatial domain method with ROI specification. The pulses were then scaled to alter the tip angle achieved, and simulated in the Bloch simulator. We calculated the average tip angle inside the resulting excited block, and NRMSE inside the

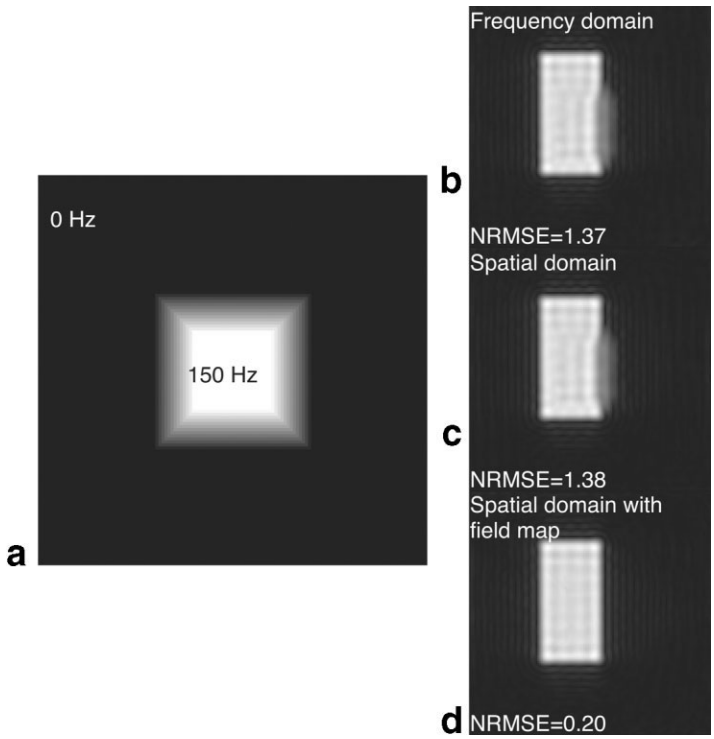

FIG. 2. **a:** Field map used in the simulation of off-resonance correction. The magnitude of the center flat region (white) is 150 Hz, while the outer region (black) is 0 Hz. **b–d:** Excitation patterns resulting from pulses designed using a speedup factor of 2, corresponding to an XFOV of 10 cm and a 3.8 ms RF pulse length. Note the distortion on the right side of the excitation pattern resulting from frequency domain-designed pulses (b) and spatial domain-designed pulses without field map incorporation (c) at this peak off-resonance.

ROI with respect to a desired pattern that was scaled to the calculated average tip angle. This process was repeated over a range of speedup factors, scaling factors, and regularization parameter values.

Scanner Experiments

We employed an experimental method based on a rearrangement of the MR signal equation to validate our pulse design method on the scanner (16). Exploiting linearity in the small-tip regime, we swapped the roles of the nonuniform transmit sensitivity patterns of the transmit coil array with the uniform receive sensitivity pattern of the body coil in the signal equation. Neglecting off-resonance and T1 and T2 decay, the signal received during readout subsequent to small-tip parallel excitation is given by a substitution of Eq. [2] into the MR signal equation:

$$s(t) = \int \left\{ i\gamma m_0(\mathbf{x}) \sum_{r=1}^{R} s_r(\mathbf{x}) \int_0^T \mathbf{b}_r(t') e^{i\gamma \mathbf{x}\cdot\mathbf{k}_i(t')} dt' \right\} e^{i\gamma \mathbf{x}\cdot\mathbf{k}_r(t)} d\mathbf{x}, \quad [7]$$

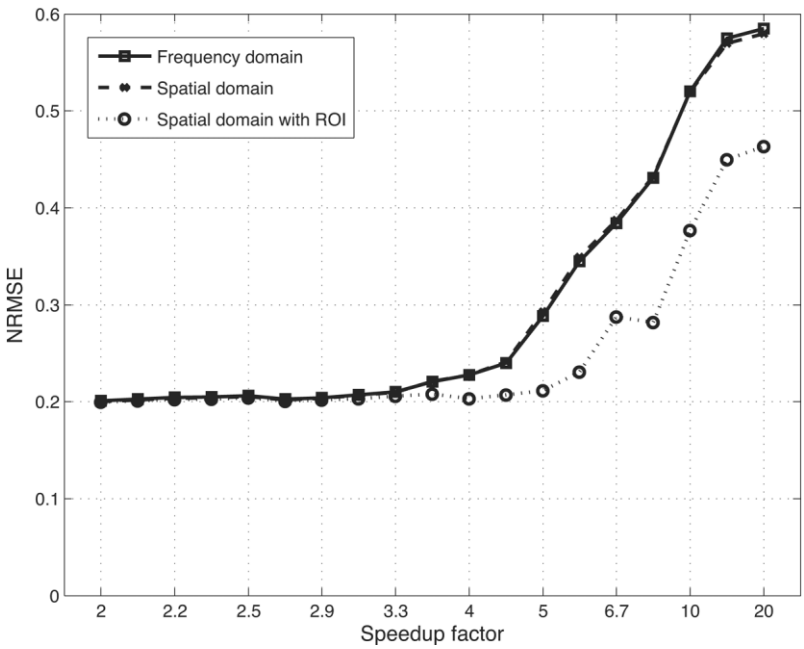

FIG. 3. Excitation error as a function of speedup factor for the three different pulse design methods. With eight coils, comparable NRMSE is achieved by the three design methods for speedup factors below 4. For speedup factors above 4, the spatial domain method with ROI specification achieves significantly lower error than the frequency domain method and the spatial domain method without ROI specification.

where $s_r(\mathbf{x})$ is coil r's transmit sensitivity pattern, and $\mathbf{k}_t(t)$ and $\mathbf{k}_r(t)$ are the transmit and receive k-space trajectories, respectively. This equation can be rearranged, bringing the summation over coils outside of the signal integral:

$$s(t) = \sum_{r=1}^{R}\left[\int s_r(\mathbf{x})\left\{ i\gamma m_0(\mathbf{x})\int_0^T \mathbf{b}_r(t')e^{i\mathbf{x}\cdot\mathbf{k}_t(t')}dt'\right\}e^{i\mathbf{x}\cdot\mathbf{k}_r(t)}d\mathbf{x}\right]. \quad [8]$$

The resulting equation demonstrates that in the case of linear small-tip excitation, the signal received subsequent to simultaneous transmission is equivalent to the signal obtained via serial transmission using each transmit coil driven in isolation, followed by a summation of the resulting signals offline, where the isolated-transmit signals are represented in Eq. [8] by the quantity inside the square brackets. Furthermore, the signal $s(t)$, is equivalent to that obtained via serial transmission using a volume coil with uniform transmit sensitivity and reception using receive coils with sensitivity patterns $s_r(\mathbf{x})$, where the excited pattern is represented in Eq. [8] by the quantity inside the curly braces. Thus, in this experiment we make use of the body coil for transmission and a head array coil for reception. The experiment proceeds as follows: the head array's receive sensitivity patterns are measured and used in the design of the parallel excitation pulses. The RF pulse designed for coil r is then played out on the body coil, and coil r is used for reception to produce an image. The process is repeated for all coils in the array, and assuming linearity under the small-tip-angle approximation, the resulting imaged excitation patterns are added together offline to obtain the final combined excitation pattern. Assuming that the receive sensitivity patterns $s_r(\mathbf{x})$ are equivalent to the transmit sensitivity patterns of some hypothetical transmit array, this method is equivalent to parallel transmission using such a transmit array. In general, this approach may not produce transmit patterns that are realizable in arbitrary objects, but it does allow for testing of the pulse design method. The procedure is useful for validating pulse design methods without requiring parallel transmit hardware that is still in the early stages of development.

We performed scanner experiments on a GE 3T Signa Excite Scanner (GE Healthcare, Milwaukee, WI, USA) using a spherical homogeneous copper sulfate phantom. The ROI, field map, and sensitivity patterns were determined from images acquired using a GRE spiral-out sequence. A spin-echo (SE) spiral-out pulse sequence was used to image excitation patterns, in which the slice-selective sinc pulse was replaced by the parallel excitation pulse. Slice selection was performed by the 180° pulse. The imaging parameters for all sequences were as follows: slice thickness = 4.0 mm, FOV = 20 cm; reconstructed matrix size = 64×64; repetition time (TR) = 2 s; echo time (TE) = 40 ms (SE) and 20 ms (GRE). Four acquisition interleaves were used in all sequences to reduce readout time and thereby minimize the effects of off-resonance during acquisition. In both experiments, the tip angles of patterns being compared were matched by normalizing parallel excitation pulses by the same value that ensured flip angles did not exceed 20°. For the parallel excitation pulses, gradient waveforms for excitation were shifted forward by 150 μs to compensate for delay between RF and gradient channels. Images were reconstructed using a fast implementation of the off-resonance compensated conjugate phase method (17). It used field maps estimated from two images acquired with a TE difference of 0.25 ms (18).

Experiment I: Off-Resonance Correction

In experiment I we validated the spatial domain method's ability to correct for distortion due to off-resonance during excitation. Three small ferromagnetic metal pieces were attached to the phantom surface to create main field inhomogeneity. With pulse lengths of 3.5 ms, 5.2 ms, and 6.9 ms, corresponding to speedup factors of 2, 4/3, and 1, pulses were designed using the spatial domain method with and without field map incorporation. The field map was estimated from two GRE images (18) with TE values of 20 ms and 20.25 ms. We masked the field map with the ROI, and then smoothed it using a regularized weighted least-squares method (15) before we incorporated it into the design process.

Experiment II: ROI Specification

In experiment II we evaluated the performance of the spatial domain method with and without ROI specification at high speedup factors. We used a speedup factor of 4, corresponding to a pulse length of 1.8 ms and XFOV of 5 cm. The resulting excitation patterns were visually compared to evaluate the performance in terms of uniformity within the excited block and erroneous excitation in the background.

RESULTS

Simulation I: Off-Resonance Correction

Figure 2 shows excitation patterns produced using the frequency domain method and the spatial domain method with and without field map incorporation. It can be seen that pulses designed using the frequency domain and spatial domain methods without field map incorporation produced distorted excitation patterns in both the transition region and the flat region of the field map, and their corresponding error is much higher than that of the spatial domain method with field map incorporation.

Simulation II: Speedup Factor

Figure 3 contains a plot of the NRMSE vs. speedup factor for the frequency domain method and the spatial domain method with and without ROI specification. All three achieved similar excitation error for speedup factors up to about 4, corresponding to an XFOV of 5 cm. However, the spatial domain method with ROI specification was able to achieve much lower error compared to the frequency domain method and the spatial domain method without ROI specification for speedup factors beyond 4. This lower error at high speedup factors for the excitation error-weighted pulses is due to an effective reduction in FOV of the desired excitation pattern via ROI specification. Figure 4 shows excitation patterns at speedup factors of 2, 4, and

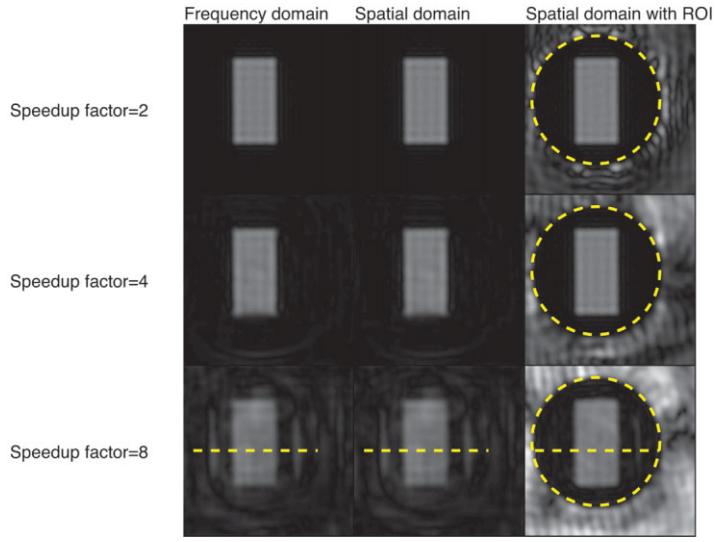

FIG. 4. Excitation patterns resulting from pulses designed for speedup factors of 8, 4, and 2. A more accurate excitation is achieved by the spatial domain method with ROI specification (indicated by dashed circle) for large speedup factors, while pulses designed using the spatial domain method without ROI specification and the frequency domain method perform similarly over the range of speedup factors. The dashed line indicates the positions of the profiles in Fig. 5. [Color figure can be viewed in the online issue, which is available at www.interscience.wiley.com.]

8. A comparison of patterns resulting from pulses designed with and without ROI specification shows that "aliased" excitation that is pushed outside the desired pattern's FOV when ROI specification *is not* used is allowed inside the desired pattern's FOV, but outside the ROI when ROI specification *is* used. The benefit of ROI specification is most visible in the patterns at a speedup factor of 8, where we can see a more accurate excitation pattern resulting from pulses designed with ROI specification than in the other two cases. Figure 5 contains profiles through the three methods' excitation patterns at this speedup factor, taken across the narrow dimension of the desired pattern and within the ROI. From this plot it is evident that, compared to the other two methods, the spatial domain method with ROI specification results in an excitation pattern that more accurately matches the desired pattern inside and outside the block.

Simulation III: Tip Angle

Figure 6 plots excitation error vs. average tip angle for pulses designed with the spatial domain method at speedup factors of 4 (Fig. 6a) and 6.7 (Fig. 6b). It can be seen that excitation accuracy degrades with increasing tip angle for both speedup factors. However, such performance degradation as a function of increasing tip angle is more rapid at high speedup factors. This is evidenced by the fact that error curves increase much more rapidly for speedup factor 6.7 than for speedup factor 4.

We find that large-tip-angle excitation error can be mitigated, particularly at high speedup factors, by increasing Tikhonov regularization in the pulse design cost function. Large Tikhonov regularization causes pulses with low integrated power to be favored in the design process over pulses with low small-tip-angle excitation error. The effi-

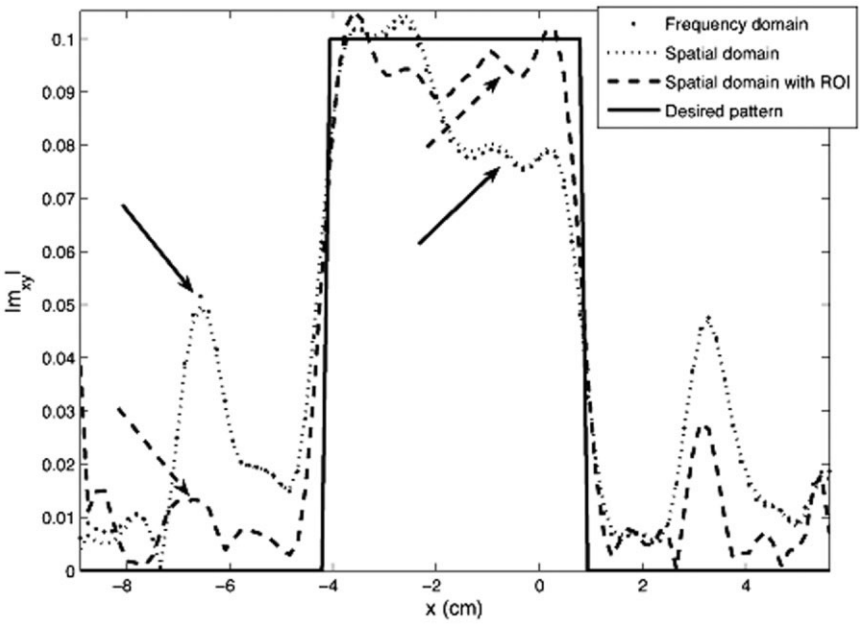

FIG. 5. Profile through the center of the excitation pattern resulting from pulses designed with speedup factor 8. A more accurate excitation across the block, as well as reduced erroneous excitation outside the block, is achieved by the spatial domain method with ROI specification. Arrows indicate areas where the spatial domain method with ROI specification (dashed arrows) achieved significantly higher accuracy than the frequency domain method and spatial domain method without ROI specification (solid arrows).

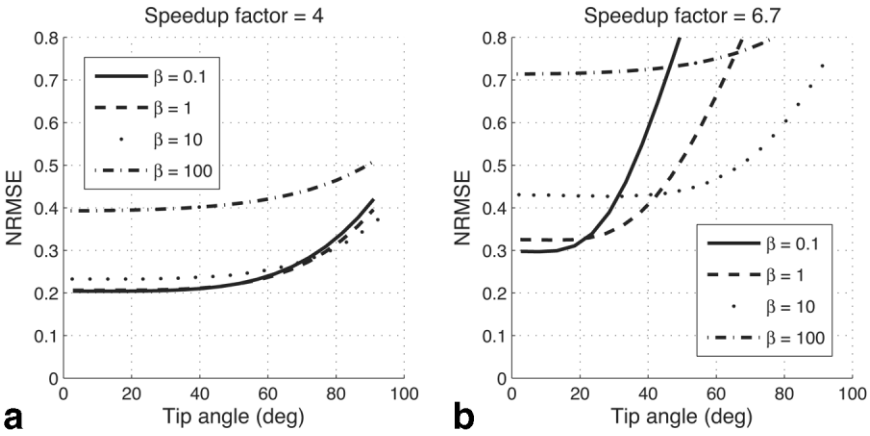

FIG. 6. Excitation error vs. average tip angle for speedup factors 4 (**a**) and 6.7 (**b**). For the lower speedup factor of 4 (a), reasonable excitation accuracy is maintained over a range of tip angles up to 90°. At a higher speedup factor of 6.7 (b), large-tip-angle performance is heavily degraded. In general, for small-tip-angle excitation, the lowest error is achieved using small Tikhonov regularization. As pulses are scaled to achieve larger tip angles, it becomes desirable to design with larger regularization. The advantage of larger regularization at large tip angles is more pronounced for high speedup factors (b) than for low speedup factors (a).

cacy of Tikhonov regularization is quantified in Fig. 6. For a relatively small speedup factor of 4 (Fig. 6a), Tikhonov regularization has some effect on large-tip-angle excitation accuracy, and it is desirable to use large β when designing for large tip angles. At a higher speedup factor of 6.7 (Fig. 6b), the effect of increased Tikhonov regularization is much more pronounced. In this case we see that for small-tip-angle excitation, it is desirable to use small β to achieve low error; however, for these values the error increases drastically with increasing tip angle. For large β, the error is higher at small tip angles, but as pulses are scaled to produce large tip angles, the error curves remain flatter, and excitation error is much lower compared to when small β is used. Figure 7 further illustrates this behavior, and shows that for speedup factor 6.7 and small Tikhonov parameter value $\beta = 0.1$, the excitation pattern becomes increasingly distorted as average tip angle increases, to the point of being unrecognizable at 90°. The erroneous excitation begins to appear around the inner perimeter of the ROI, in areas of high transmit sensitivity pattern magnitude. In contrast, pulses designed with larger β produce patterns with reduced distortion at 90°, with the best accuracy attained using the largest Tikhonov parameter value simulated, $\beta = 100$. For a 45° tip angle, though, $\beta = 10$ provides the best accuracy, indicating that the best choice of β is a function of tip angle.

Experiment I: Off-Resonance

The estimated field map (Fig. 8a) revealed global field distortion caused by the attached metal, with a maximum field offset of 150 Hz occurring in the lower left side of the slice of interest. Figure 8b shows the resulting excitation patterns from pulses designed both with and without off-resonance incorporation in the design, at three different speedup factors of 2, 4/3, and 1, corresponding to pulse lengths of 3.5 ms, 5.2 ms, and 6.9 ms. With increasing pulse length, off-resonance during excitation results in excitation patterns with an increasingly distorted and blurred lower-left corner when a field map is not incorporated into the design. When a field map is used, however, the definition of the excitation pattern is maintained with increasing pulse length, and erroneous excitation outside the block is reduced due to the decreasing speedup factor.

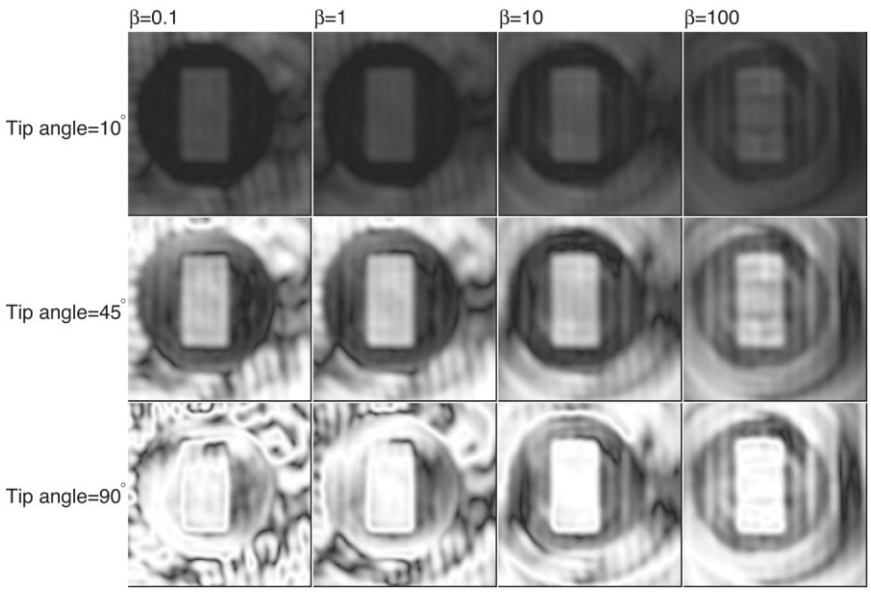

FIG. 7. Tikhonov regularization parameter vs. tip angle for speedup factor 6.7. Increasing the Tikhonov regularization (β) in the cost function improves excitation accuracy at large tip angles. Tip angles are calculated as the average tip angle over the region corresponding to the desired excitation pattern.

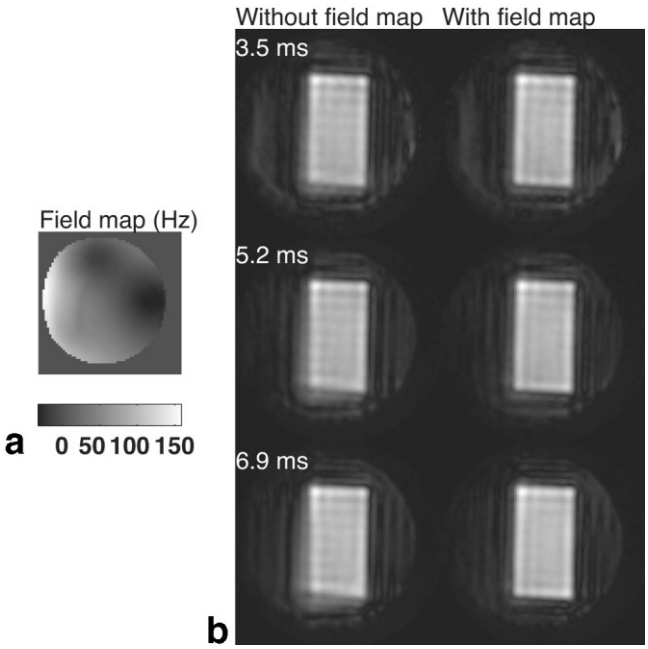

FIG. 8. Excitation patterns (**b**) resulting from pulses designed with and without incorporation of a field map (**a**) for pulse lengths of 3.5 ms (speedup factor 2), 5.2 ms (speedup factor 4/3), and 6.9 ms (speedup factor 1). Pulses designed without field map incorporation yielded excitation patterns with increasing blur with respect to pulse length, while pulses designed with field map incorporation yielded excitation patterns that remained well defined over all pulse lengths.

Experiment II: ROI Specification

Incorporating the ROI (Fig. 9a) into the design process results in higher excitation accuracy within the ROI. Figure 9b shows the excitation patterns resulting from pulses designed with and without ROI specification. The pattern with ROI specification is more uniform over the block, and contains less erroneous excitation around the perimeter of the block. Thus, ROI specification results in a more accurate excitation pattern at this speedup factor of 4.

DISCUSSION AND CONCLUSIONS

In this work we have presented a spatial domain method for designing RF pulses in multicoil parallel excitation, and verified it with both simulations and MR phantom experiments. The new design method is formulated as a minimization problem in which the resulting RF pulses are the minimizer of a quadratic cost function comprising a weighted norm-squared error term and regularization terms, the latter of which may be used to control integrated and peak RF power. The minimization problem may be solved iteratively via the CG method or brute-force inversion.

In some cases the new design approach produces RF pulses similar in quality to those obtained by the frequency domain method of transmit SENSE (1), e.g., in the special case that Tikhonov regularization is used, but neither ROI specification nor main field inhomogeneity compensation are incorporated in the design process. In general, though, it has some important advantages over that method. It allows for a spatially varying excitation error weighting, such as ROI specification, which we have shown leads to increased excitation accuracy at high speedup factors. This is because error outside the ROI does not contribute to the norm-squared error term of the design cost function, providing more degrees of freedom to achieve higher excitation accuracy inside the ROI. ROI specification effectively decreases the FOV of the desired excitation pattern, and thus decreases the effective speedup factor. In a given imaging experiment, an ROI can be determined automatically in the pulse design process by thresholding prescan images obtained for sensitivity mapping to yield an ROI corresponding to spatial locations containing tissue. The new design method also allows for compensation of magnetic field inhomogeneities via incorporation of an extra phase term in the design system matrix, which we have shown in our simulations and experiments increases excitation accuracy in the presence of magnetic field inhomogeneities, by allowing each spatial point to effectively experience a unique *k*-space trajectory. In experiment I it was shown that in the presence of field inhomogeneities, the new method maintains excitation accuracy at lower speedup factors, compared to methods that do not account for the effects of off-resonance. The method does not require computation of *k*-space traversal speed and density compensation functions, nor does it require interpolation in the design process, unlike the method of Ref. 1. In contrast to the design methods proposed in Refs. 2 and 3, the new design approach allows the use of arbitrary *k*-space trajectories and provides additional design controls. Though not presented here, simulations performed using an EPI trajectory yielded results consistent with those obtained using a spiral trajectory.

We also investigated the behavior, in terms of excitation accuracy, of pulses designed using the proposed method as they are scaled to produce tip angles up to 90°. It was shown that excitation patterns became heavily distorted at these tip angles due to Bloch equation nonlinearity, and

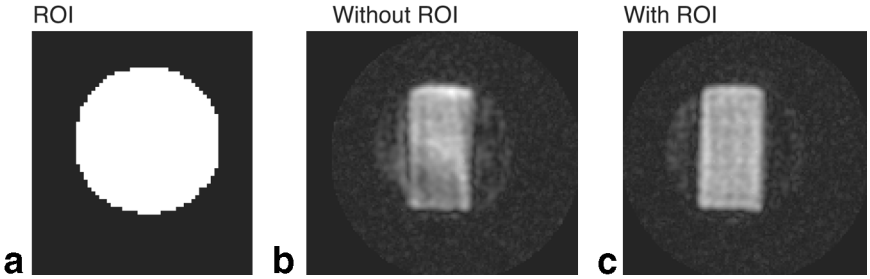

FIG. 9. **a:** ROI defined by thresholding the body coil image. At a speedup factor of 4, incorporation of ROI (**c**) resulted in improved uniformity inside the block, and suppressed error in the background, compared to pulses designed without ROI specification (**b**).

that the distortion becomes worse as the speedup factor is increased. One interpretation of this result is that at high speedup factors XFOV is small, and each coil plays an increased role in canceling aliased excitation produced by other coils. Thus, the individual coil excitation patterns are less localized, and each coil excites larger tip angles over a larger region of space compared to small speedup factors. As pulses are scaled up, the largest tip angles in the individual coil excitation patterns leave the small-tip-angle regime earliest and fail to combine effectively to cancel aliased excitation, thereby producing the observed distortion. Thus, the linear small-tip-angle assumption that the total tip angle produced by each individual coil commutes with the tip angles produced by the other coils is broken. A second interpretation is lent by the analysis used to derive the linear class of large-tip-angle pulses (19). Pulses of this class may be linearly scaled to produce large tip angles, provided that they meet three conditions: 1) the deposition of energy in *k*-space is Hermitian symmetric, 2) the RF magnitude is approximately zero compared to the gradient field magnitude, and 3) the excitation *k*-space trajectory may be approximately decomposed into individually refocused trajectories. In our tip angle simulation, *k*-space energy deposition is approximately Hermitian symmetric, so the first condition is met. However, at high speedup factors in parallel excitation, *k*-space coverage is sparse, which results in increased RF magnitude, so the second approximation becomes inaccurate. Also, at high speedup factors the distance between individual spiral arcs increases, so the third approximation also becomes inaccurate. In the simulation we demonstrated the utility of Tikhonov regularization in mitigating increased excitation error at large tip angles and high speedup factors. The demonstrated error behavior with respect to Tikhonov regularization parameter may be understood from the first perspective above by considering that increasing the parameter in the design process causes pulses with low integrated RF power to be favored over those with low norm-squared excitation error. These pulses produce individual coil excitation patterns that have smaller tip angles in general, but whose combination still yields the desired average excited tip angle. Because these pulses combine more constructively, they are less susceptible to the adverse effects of Bloch equation nonlinearity. Thus, combination and aliased excitation cancellation performance is relatively well maintained as they are scaled to produce large tip angles. From the linear class perspective, Tikhonov regularization results in pulses with lower magnitude, and thus the second approximation is more accurate when it is used. Thus, we conclude that at high speedup factors and large tip angles, it is desirable in terms of excitation error to use a large Tikhonov regularization parameter. Although the appropriate choice of Tikhonov parameter is complicated by the nonlinear nature of the effect we wish to mitigate, we have found that a metric that quantifies the inaccuracy of the second approximation of the linear class formulation can be useful for predicting the accuracy of a given pulse at large tip angles, and may thus serve as a guideline for choosing an appropriate parameter. The metric we tested was the average, over the pulse duration, of the ratio of instantaneous total RF magnitude (averaged over the sample) to gradient magnitude, and we found that the larger this metric, the more inaccurate pulses are as they are scaled to large tip angles. One could incorporate this metric into a practical imaging experiment by initially designing pulses with a small Tikhonov regularization parameter, and repeating the pulse design process with larger parameters until the metric falls below a certain "safe" number, the value of which may be a function of the desired excitation pattern, *k*-space trajectory, and tip angle. In general, though, while we have shown that acceleration worsens the large tip-angle performance of small-tip-designed pulses, the results presented here are still surprisingly good for a range of speedup factors.

APPENDIX

The transmit SENSE (1) approach to RF pulse design in parallel excitation is formulated in the frequency, or *k*-space domain. Assuming small tip angles, the Fourier transform of an excitation pattern $\mathbf{m}(\mathbf{x})$ resulting from simultaneous excitation by R coils is given by:

$$p(\mathbf{k}) = \sum_{r=1}^{R} S_r(\mathbf{k}) \otimes p_r(\mathbf{k}), \qquad [9]$$

where S_r is the Fourier transform of the transmit sensitivity pattern of coil r, p_r is the Fourier transform of the excitation pattern produced by coil r, and the operator $\otimes$ denotes a convolution. This equation may be discretized in $\mathbf{k}$, forming vectors from p and p_r, and circulant convolution matrices from samples of S_r. A regularized least-squares cost function may then be formed and minimized to yield the Fourier transforms of the individual coils' excitation patterns:

$$\Psi_{fd}(\mathbf{p}_{full}) = \|\mathbf{S}_{full}\mathbf{p}_{full} - \mathbf{p}_{des}\|^2 + \beta\|\mathbf{p}_{full}\|^2, \qquad [10]$$

$$\mathbf{p}_{full} = [\ \mathbf{p}_1 \quad \cdots \quad \mathbf{p}_R\ ]^T,$$

$$\mathbf{S}_{full} = [\ \mathbf{S}_1 \quad \cdots \quad \mathbf{S}_R\ ],$$

where $\mathbf{p}_{des}$ is a vector containing samples of the Fourier transform of the desired excitation pattern. The $\mathbf{p}_{full}$ that minimizes Eq. [10] is

$$\hat{\mathbf{p}}_{full} = (\mathbf{S}'_{full}\mathbf{S}_{full} + \beta\mathbf{I})^{-1}\mathbf{S}'_{full}\mathbf{p}_{des}$$

$$= \mathbf{S}'_{full}(\mathbf{S}_{full}\mathbf{S}'_{full} + \beta\mathbf{I})^{-1}\mathbf{p}_{des}, \qquad [11]$$

where we have used the "push-through" matrix identity. Thus, for coil r, the minimizing $\mathbf{p}_r$ is given by

$$\mathbf{p}_r = \mathbf{S}'_r(\mathbf{S}_{full}\mathbf{S}'_{full} + \beta\mathbf{I})^{-1}\ \mathbf{p}_{des}. \qquad [12]$$

The RF pulse for the r-th coil, $\mathbf{b}_r$, can be derived from $\mathbf{p}_r$ by multiplication with the Jacobian determinant for *k*-space density and velocity compensation (1).

The spatial domain and frequency domain methods are approximately equivalent when neither ROI nor magnetic

field inhomogeneity compensation are incorporated into the design process, and when Tikhonov regularization that penalizes integrated RF power is used. In this special case, the cost function for the spatial domain method is

$$\Psi_{sd}(\mathbf{b}_{full}) = \|\mathbf{A}_{full}\mathbf{b}_{full} - \mathbf{m}_{des}\|^2 + \beta\|\mathbf{b}_{full}\|^2, \quad [13]$$

and the $\mathbf{b}_r$ that minimizes this cost function is given by

$$\mathbf{b}_r = \mathbf{A}'\mathbf{D}_r'(\mathbf{A}_{full}\mathbf{A}'_{full} + \beta\mathbf{I})^{-1}\mathbf{m}_{des}. \quad [14]$$

The matrix product $\mathbf{A}_{full}\mathbf{A}'_{full}$ is equal to a summation over coils of the product of the diagonal sensitivity matrices $\mathbf{D}_r$ with the system matrix $\mathbf{A}$, times its conjugate transpose:

$$\mathbf{A}_{full}\mathbf{A}'_{full} = \sum_{r=1}^{R}\mathbf{D}_r\mathbf{A}\mathbf{A}'\mathbf{D}_r'. \quad [15]$$

The (j,k)-th element of the matrix $\mathbf{AA}'$ is given by

$$[\mathbf{AA}']_{j,\,k} = \sum_{i=1}^{N_k} e^{i\mathbf{k}_j(\mathbf{x}_j - \mathbf{x}_k)}. \quad [16]$$

Assuming Cartesian sampling in space, this matrix is Toeplitz, and is approximately circulant (20). This allows us to write

$$\mathbf{AA}' \approx \mathbf{Q}'\mathbf{H}\mathbf{Q}, \quad [17]$$

where $\mathbf{H}$ is a diagonal matrix containing samples of the DFT of the first column of $\mathbf{AA}'$, and $\mathbf{Q}, \mathbf{Q}'$ are orthonormal forward and inverse DFT matrices, respectively. We may then substitute this expansion into the solution for the RF pulse of coil r. At the same time, we insert DFT matrices on both sides of $\mathbf{D}_r$ and on the left of $\mathbf{m}_{des}$, which is allowed since $\mathbf{Q}'\mathbf{Q} = \mathbf{I}$, yielding

$$\mathbf{b}_r \approx \mathbf{A}'\mathbf{Q}'\mathbf{Q}\mathbf{D}_r'\mathbf{Q}'\mathbf{Q}\left(\sum_{r=1}^{R}\mathbf{D}_r\mathbf{Q}'\mathbf{H}\mathbf{Q}\mathbf{D}_r' + \beta\mathbf{I}\right)^{-1}\mathbf{Q}'\mathbf{Q}\mathbf{m}_{des}. \quad [18]$$

We bring these DFT matrices into the inverse, yielding

$$\mathbf{b}_r \approx \mathbf{A}'\mathbf{Q}'\tilde{\mathbf{S}}_r'\left(\sum_{r=1}^{R}\tilde{\mathbf{S}}_r\mathbf{H}\tilde{\mathbf{S}}_r' + \beta\mathbf{I}\right)^{-1}\mathbf{Q}\mathbf{m}_{des}, \quad [19]$$

where $\tilde{\mathbf{S}}_r = \mathbf{Q}\mathbf{D}_r\mathbf{Q}'$. The $\mathbf{Q}$ on the right side of this expression has the effect of transforming the desired excitation pattern into the frequency domain, and the product $\mathbf{A}'\mathbf{Q}'$ on the left side has the effect of performing Cartesian to k-space trajectory interpolation and multiplication by the Jacobian determinant. The circulant convolution matrix $\tilde{\mathbf{S}}_r$ is defined on a Cartesian grid of frequency locations, and thus the product $\mathbf{A}'\mathbf{Q}'\tilde{\mathbf{S}}_r'$ represents the combined action of the matrix $\mathbf{S}_r'$ in Eq. [11] and multiplication by the Jacobian determinant. Furthermore, $\sum_{r=1}^{R}\tilde{\mathbf{S}}_r\mathbf{H}\tilde{\mathbf{S}}_r' \approx \mathbf{S}_{full}\mathbf{S}'_{full}$, and $\mathbf{Q}\mathbf{m}_{des} = \mathbf{p}_{des}$. Thus this final expression is equivalent to that for the minimizing RF pulse for coil r in the frequency domain method of transmit SENSE (1), under the approximation in Eq. [17]. This approximate equivalence is established under the special conditions that neither ROI nor main field inhomogeneity compensation are incorporated into the design process, and that Tikhonov regularization is used.

REFERENCES

1. Katscher U, Bornert P, Leussler C, van den Brink JS. Transmit SENSE. Magn Reson Med 2003;49:144–150.
2. Zhu Y. Parallel excitation with an array of transmit coils. Magn Reson Med 2004;51:775–784.
3. Griswold M, Kannengiesser S, Muller M, Jakob P. Autocalibrated accelerated parallel excitation (transmit-GRAPPA). In: Proceedings of the 13th Annual Meeting of ISMRM, Miami Beach, FL, USA, 2005. p 2435.
4. Pruessmann KP, Weiger M, Scheidegger MB, Boesiger P. SENSE: sensitivity encoding for fast MRI. Magn Reson Med 1999;42:952–962.
5. Griswold MA, Jakob PM, Heidemann RM, Nittka M, Jellus V, Wang J, Kiefer B, Haase A. Generalized autocalibrating partially parallel acquisitions (GRAPPA). Magn Reson Med 2002;47:1202–1210.
6. Pauly J, Nishimura D, Macovski A. A k-space analysis of small-tip-angle excitation. J Magn Reson 1989;81:43–56.
7. Saekho S, Boada FE, Noll DC, Stenger VA. Small tip angle three-dimensional tailored radiofrequency slab-select pulse for reduced B1 inhomogeneity at 3 T. Magn Reson Med 2005;53:479–484.
8. Stenger VA, Saekho S, Zhang Z, Yu S, Boada FE. B1 inhomogeneity reduction with transmit SENSE. In: Proceedings of the 2nd International Workshop on Parallel MRI, Zurich, Switzerland, 2004. p 94.
9. Katscher U, Vernickel P, Hanft M. Static and dynamic RF-shimming in the framework of transmit SENSE. In: Proceedings of the 13th Annual Meeting of ISMRM, Miami Beach, FL, USA, 2005. p 2256.
10. Stenger VA, Boada FE, Noll DC. Three-dimensional tailored RF pulses for the reduction of susceptibility artifacts in T_2^*-weighted functional MRI. Magn Reson Med 2000;44:525–531.
11. Zhu Y, Watkins R, Giaquinto R, Hardy C, Kenwood G, Mathias S, Valent T, Denzin M, Hopkins J, Peterson W, Mock B. Parallel excitation on an eight transmit-channel MRI system. In: Proceedings of the 13th Annual Meeting of ISMRM, Miami Beach, FL, USA, 2005. p 14.
12. Ullmann P, Junge S, Wick M, Seifert F, Ruhm W, Hennig J. Experimental analysis of parallel excitation using dedicated coil setups and simultaneous RF transmission on multiple channels. Magn Reson Med 2005;54:994–1001.
13. Yip CY, Fessler JA, Noll DC. Iterative RF pulse design for multidimensional, small-tip-angle selective excitation. Magn Reson Med 2005;54:908–917.
14. Sutton BP, Noll DC, Fessler JA. Fast, iterative image reconstruction for MRI in the presence of field inhomogeneities. IEEE Trans Med Imaging 2003;22:178–188.
15. Fessler JA, Yeo D, Noll DC. Regularized fieldmap estimation in MRI. In: Proceedings of the IEEE International Symposium on Biomedical Imaging, Arlington, VA, USA, 2006. p 1015.
16. Zhang Z, Stenger VA. Validation of transmit SENSE with reciprocity. In: Proceedings of the 13th Annual Meeting of ISMRM, Miami Beach, FL, USA, 2005. p 2434.
17. Noll DC, Meyer CH, Pauly J, Nishimura D, Macovski A. A homogeneity correction method for magnetic resonance imaging with time-varying gradients. IEEE Trans Med Imaging 1991;10:629–637.
18. Schneider E, Glover G. Rapid in vivo proton shimming. Magn Reson Med 1991;18:335–347.
19. Pauly JM, Nishimura DG, Macovski A. A linear class of large-tip-angle selective excitation pulses. J Magn Reson 82:571–587, 1989.
20. Chan RH, Ng MK. Conjugate gradient methods for Toeplitz systems. SIAM Rev 1996;38:427–482.